applied sciences

MDPI

Article

Intramolecular Spin State Locking in Iron(II) 2,6-Di(pyrazol-3-yl)pyridine Complexes by Phenyl Groups: An Experimental Study

Yulia Nelyubina [1,2,*], Alexander Polezhaev [1,3], Alexander Pavlov [1], Dmitrii Aleshin [1,4], Svetlana Savkina [1], Nikolay Efimov [2], Teimur Aliev [1] and Valentin Novikov [1,*]

[1] A.N. Nesmeyanov Institute of Organoelement Compounds, Vavilova Str. 28, 119991Moscow, Russia; aleksandr.polejaev@gmail.com (A.P.); pavlov@ineos.ac.ru (A.P.); dima.aleshin26@gmail.com (D.A.); savkinasveta91@mail.ru (S.S.); a.teimur1990@gmail.com (T.A.)
[2] Kurnakov Institute of General and Inorganic Chemistry, Leninsky prosp. 31, 119991 Moscow, Russia; nnefimov@yandex.ru
[3] Bauman Moscow State Technical University, 2nd Baumanskaya Str. 5, 105005 Moscow, Russia
[4] Lomonosov Moscow State University, Leninskiye Gory, 1, 119991 Moscow, Russia
* Correspondence: unelya@ineos.ac.ru (Y.N.); novikov84@ineos.ac.ru (V.N.); Tel.: +7-499-135-6568 (N.Y)

Received: date; Accepted: date; Published: date

Table S1. Crystal data and structure refinement parameters for the studied complexes.

Parameter	**$Fe(L1)_2OTf_2$**	**$Zn(L1)_2(ClO_4)_2$.**	**$Fe(L2)_2OTf_2$**	**$Fe(L2)_2(BF_4)_2$**
Formula unit	$C_{46}H_{34}FeN_{10}O_4$, $2CF_3O_3S$, $C_4H_{10}O$	$4C_{46}H_{34}N_{10}O_4Zn$, $8ClO_4$, $4C_4H_{10}O$, $7C_2H_3N$, $16H_2O$	$2C_{54}H_{42}FeN_{10}O_8$, $4CF_3O_3S$, $2CH_2Cl_2$, $3.5H_2O$	$C_{54}H_{42}FeN_{10}O_8$, $2BF_4$, $2CH_2Cl_2$
Formula weight	1218.94	5092.51	2858.83	1358.30
Crystal system	Monoclinic	Monoclinic	Triclinic	Monoclinic
Space group	$P2_1/n$	$P2_1/c$	P-1	$P2_1$
Z	4	1	1	2
a, Å	15.7804(11)	15.5731(6)	13.5638(17)	12.3685(9)
b, Å	21.7218(15)	15.7187(6)	13.8402(17)	19.7935(15)
c, Å	16.0669(12)	24.4975(9)	19.155(2)	13.5108(10)
α, °	90	90	103.274(2)	90
β, °	102.990(2)	105.3980(10)	100.382(2)	116.8220(10)
γ, °	90	90	113.756(2)	90
V, $Å^3$	5366.5(7)	5781.5(4)	3049.5(7)	2951.8(4)
D_{calc} (g cm^{-1})	1.509	1.463	1.557	1.528
Linear absorption,	4.5	5.98	4.99	5.26

μ (cm^{-1})				
F(000)	2504	2642	1463	1384
$2\Theta_{max}$, °	54	56	52	54
Reflections measured	55433	64424	38944	52651
Independent reflections	11726	13975	11988	12890
Observed reflections [$I > 2\sigma(I)$]	8202	10262	5969	10532
Parameters	743	808	851	807
R1	0.0904	0.0567	0.0916	0.0470
wR2	0.2474	0.1839	0.2593	0.1146
GOF	1.399	1.147	1.141	1.002
$\Delta\rho_{max}/\Delta\rho_{min}$ (e Å^{-3})	0.979/-0.579	1.253/-0.784	1.523/-1.315	0.482/-0.382

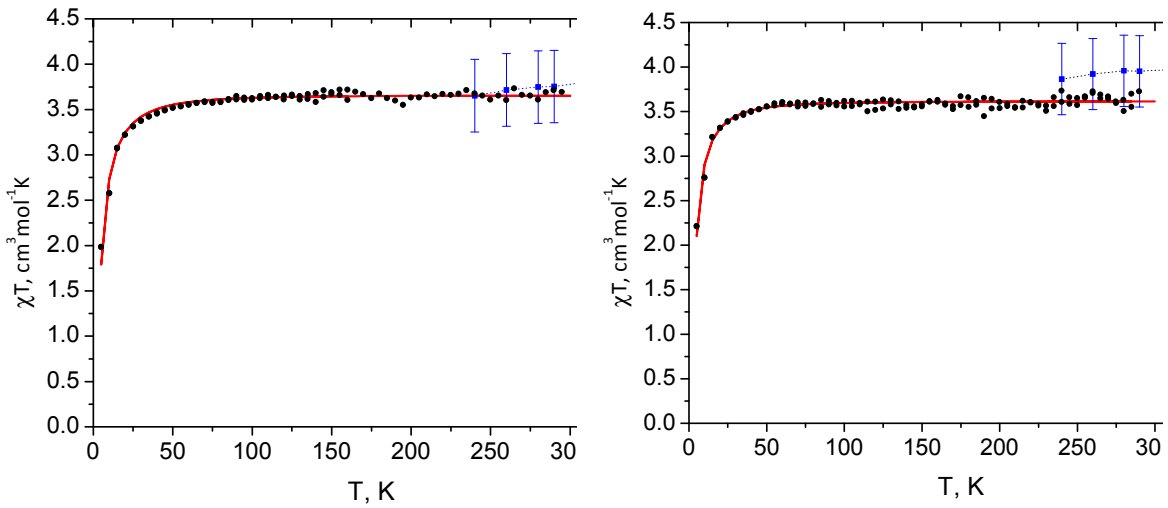

Figure S1. Variable-temperature magnetic susceptibility data for microcrystalline samples of Fe(**L2**)$_2$OTf$_2$ (**a**) and Fe(**L2**)$_2$(BF$_4$)$_2$ (**b**) according to *dc*-magnetometry (●) and for their acetonitrile-d$_3$ solutions according to the Evans method (■). The red line represents the fit.

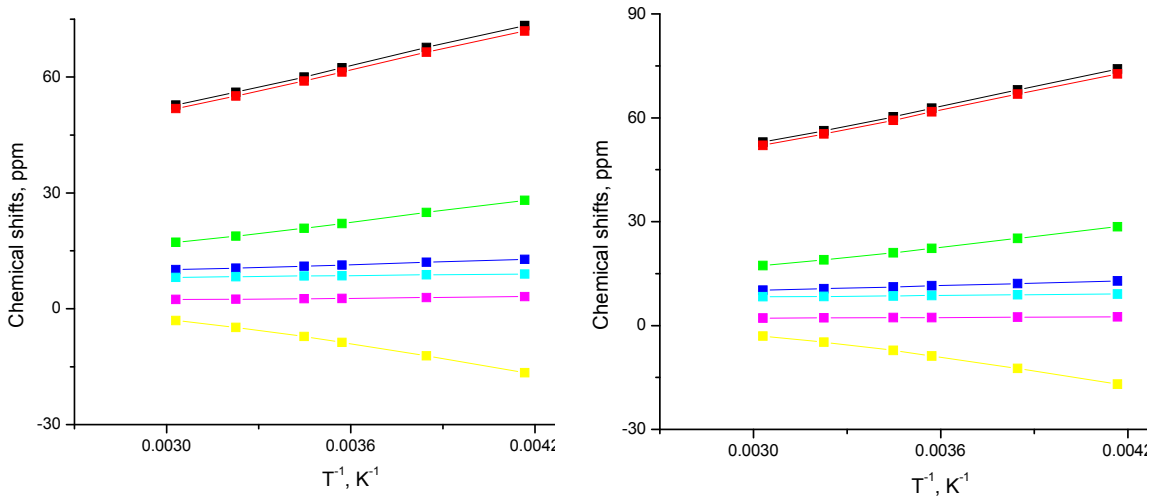

(**a**) (**b**)

Figure S2. ^{1}H chemical shifts for an acetonitrile-d$_3$ solution of Fe(**L2**)$_2$OTf$_2$ (**a**) and Fe(**L2**)$_2$(BF$_4$)$_2$ (**b**) plotted versus *1/T*. The solid lines represent linear fits.

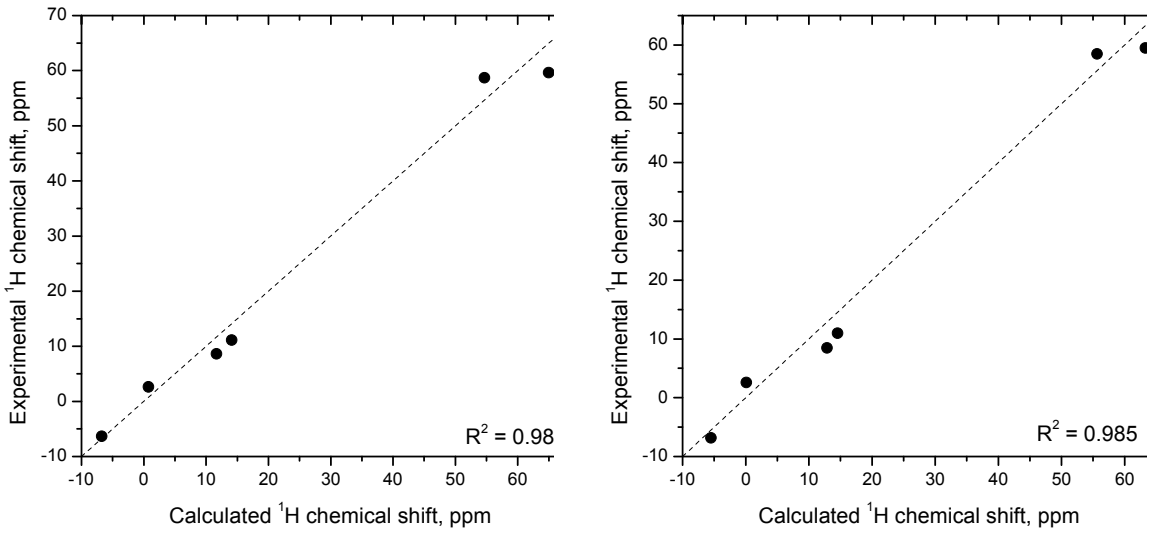

(**a**) (**b**)

Figure S3. Correlation plot of experimental *vs.* theoretical ^{1}H chemical shifts for Fe(**L2**)$_2$OTf$_2$ with optimized (**a**) and X-ray geometries (**b**) of [Fe(**L2**)$_2$]$^{2+}$; $\Delta\chi_{ax}$ = 7.61·10^{-32} m^3.

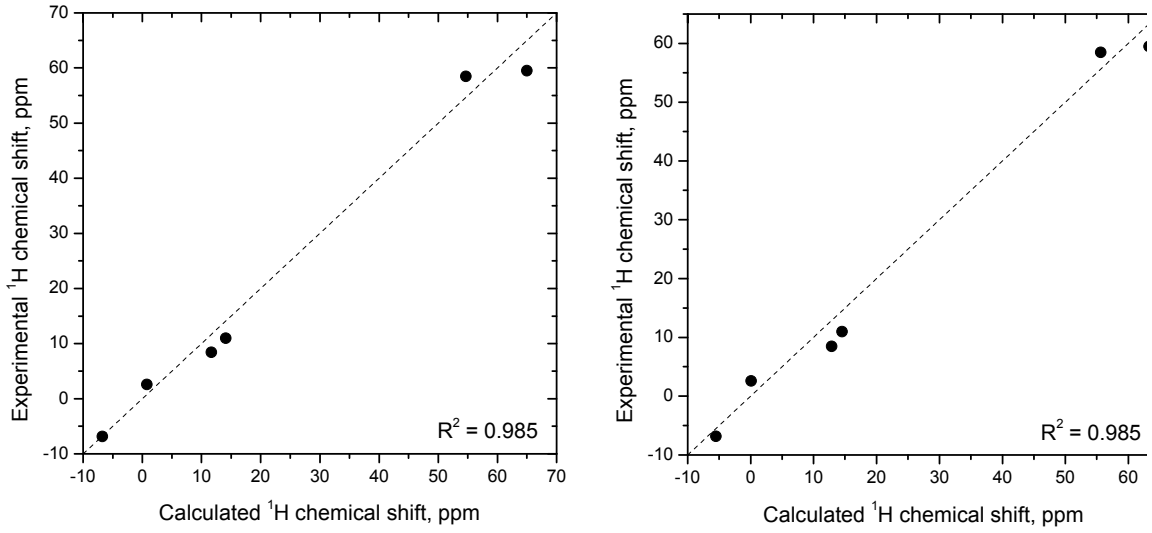

(**a**) (**b**)

Figure S4. Correlation plot of experimental *vs.* theoretical ^{1}H chemical shifts for Fe(**L2**)$_2$(BF$_4$)$_2$ with optimized (**a**) and X-ray geometries (**b**) of [Fe(**L2**)$_2$]$^{2+}$; $\Delta\chi_{ax}$ = 7.61·10^{-32} m^3.

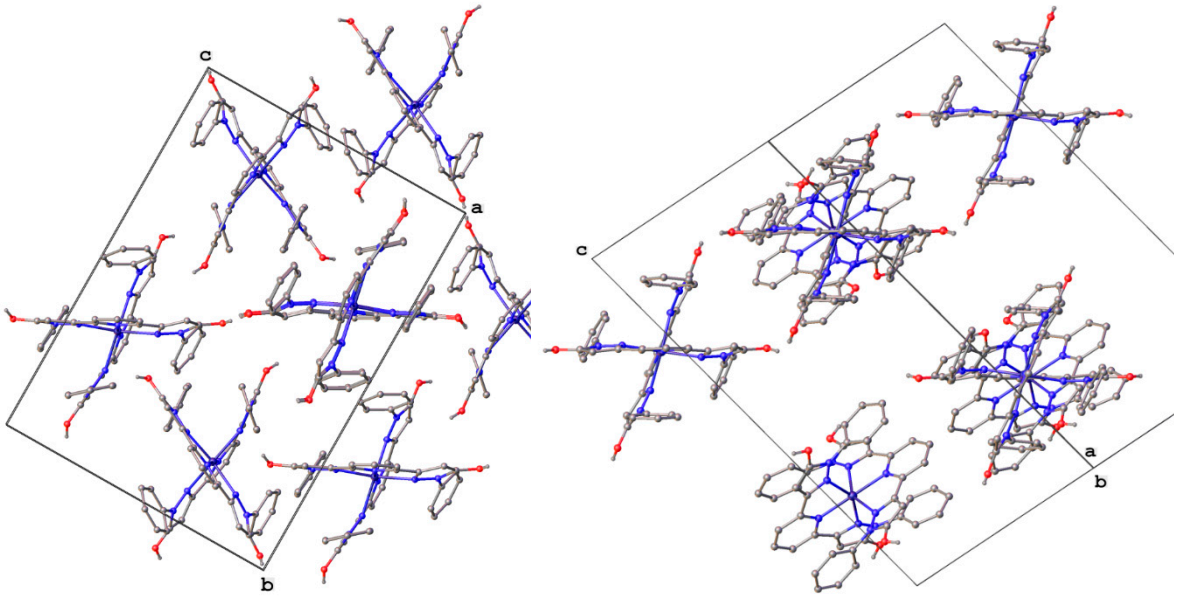

(**a**) (**b**)

Figure S5. Packing of [ML$_2$]$^{2+}$ cations in Fe(**L1**)$_2$OTf$_2$ (**a**) and Zn(**L1**)$_2$(ClO$_4$)$_2$ (**b**).

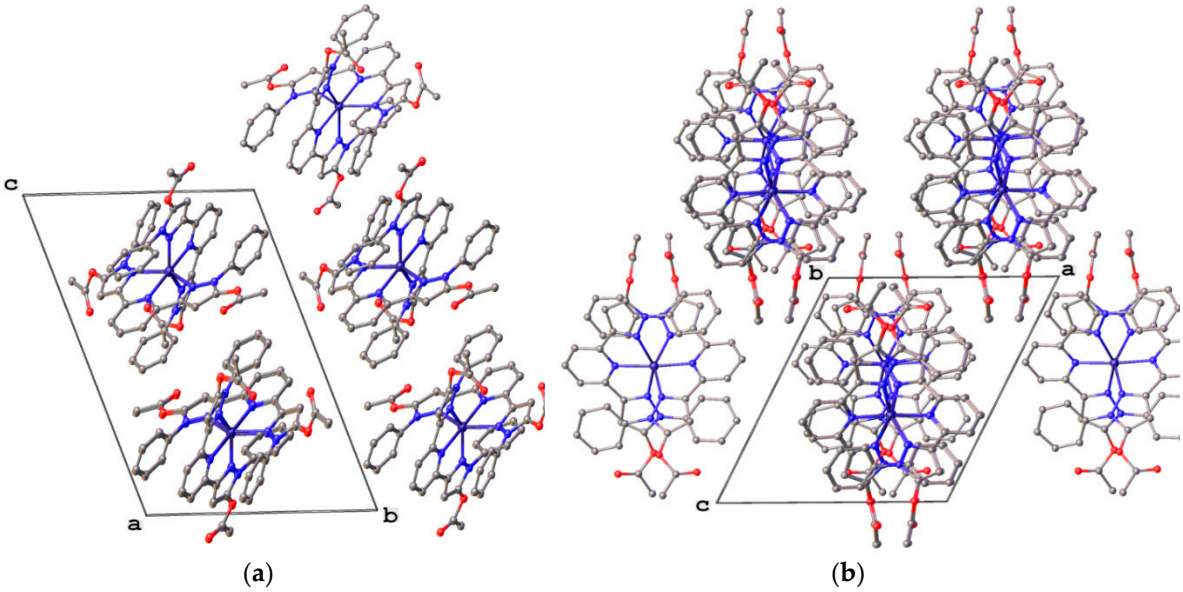

Figure S6. Packing of $[ML_2]^{2+}$ cations in Fe(**L2**)$_2$OTf$_2$ (**a**) and Fe(**L2**)$_2$(BF$_4$)$_2$ (**b**).

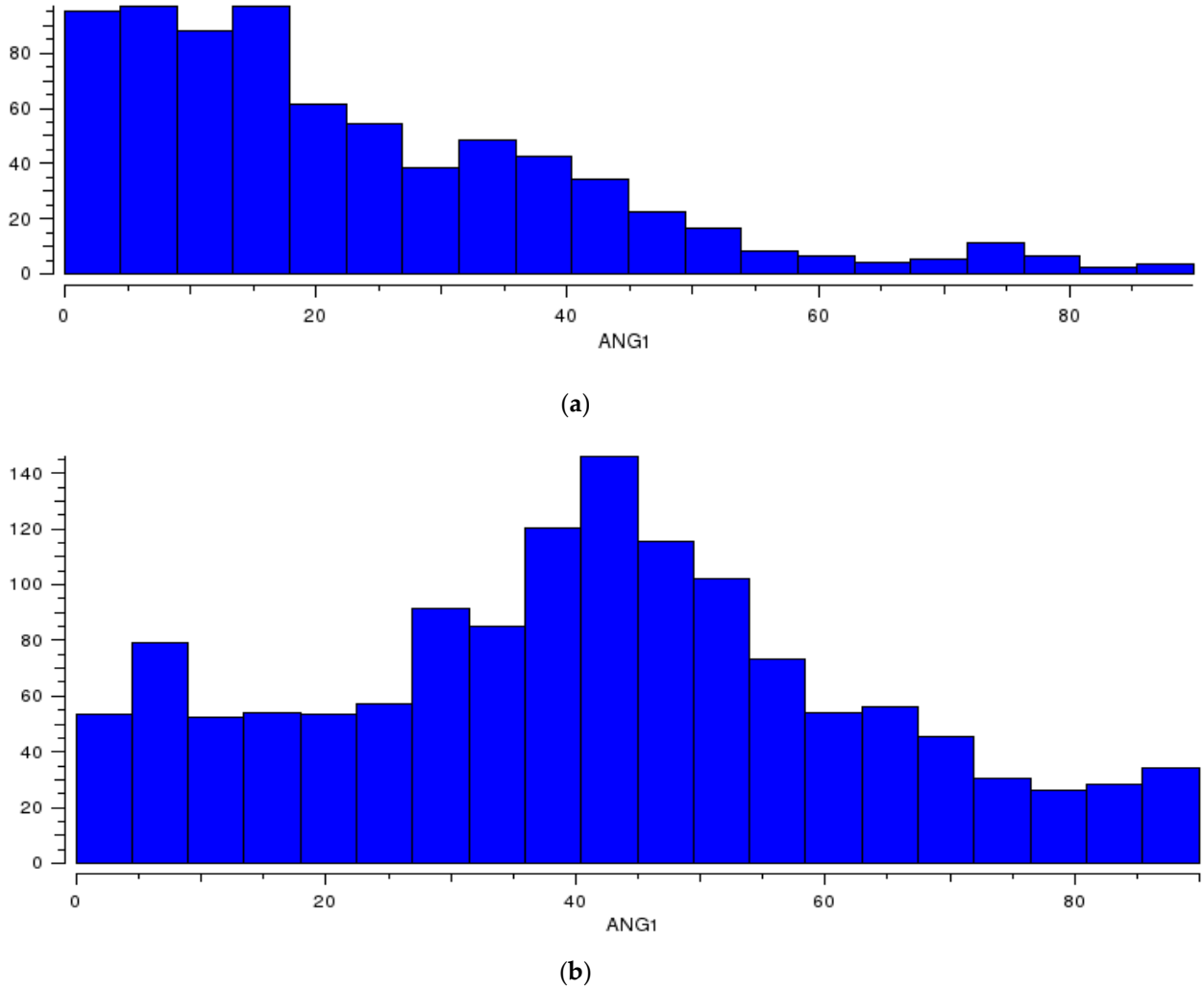

Figure S7. Organic compounds with a phenyl-pyrazol-1-yl (**a**) or phenyl-pyrazol-3-yl (**b**) fragment distributed over the the angle between the two planes.

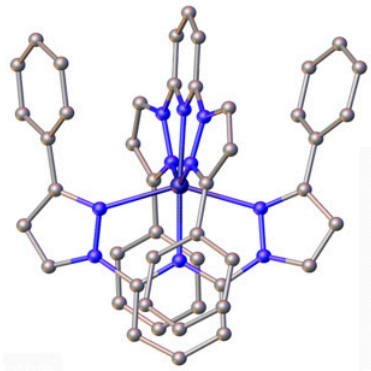

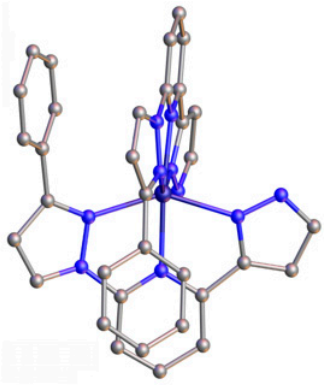

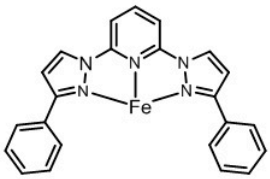

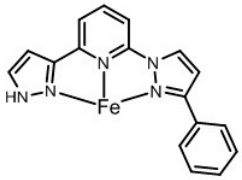

$[Fe(Ph_2\text{-}1\text{-}bpp)_2]^{2+}$		$[Fe(Ph\text{-}1,3\text{-}bpp)_2]^{2+}$	
Spin state	HS	Spin state	HS
θ,°	61.2-62.3	θ,°	69.8-71.5
γ,°	32.4 – 36.5	γ,°	45.3 – 49.2

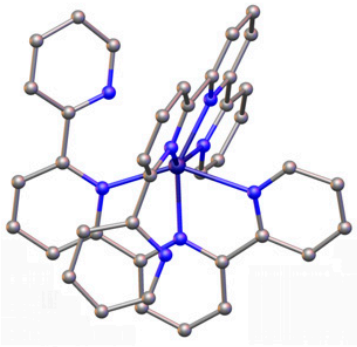

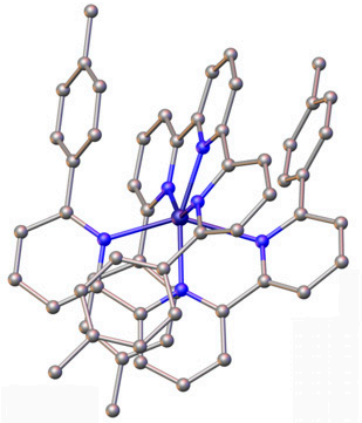

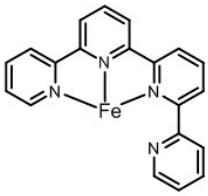

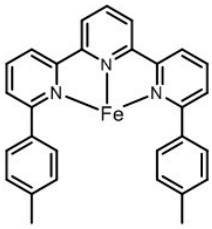

$[Fe(Py\text{-}tpy)_2]^{2+}$		$[Fe(pTol_2\text{-}tpy)_2]^{2+}$	
Spin state	HS	Spin state	HS
θ,°	76.5	θ,°	58.8°
γ,°	68.8	γ,°	39.7 – 52.9

Figure S8. General view of the HS complexes $[Fe(L)_2]^{2+}$ of terpy (above) and bpp (below) with phenyl groups (and similar) from CSD showing 'parallel-displaced' intramolecular stacking interactions, and their schematic representation.

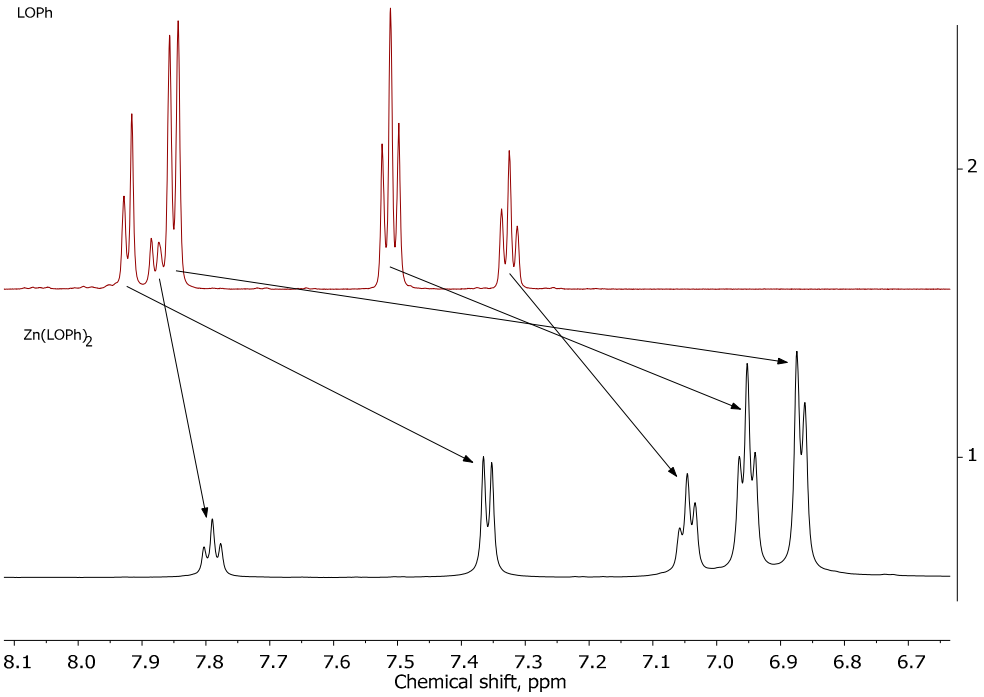

Figure S9. ^{1}H NMR spectra of the ligand **L1** (above) and the complex Zn(**L1**)$_2$(ClO$_4$)$_2$ (below).

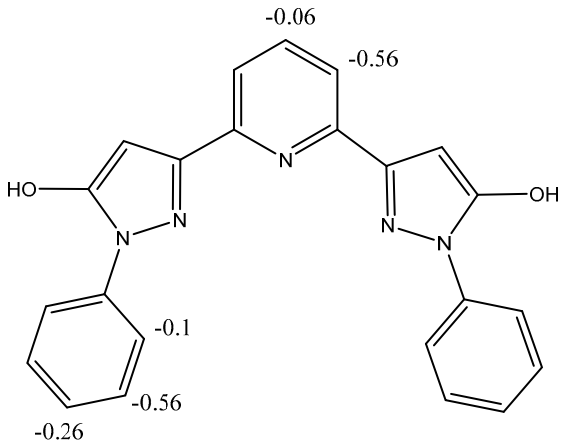

Figure S10. Differences in ^{1}H chemical shifts between the complex Zn(**L1**)$_2$(ClO$_4$)$_2$ and the ligand **L1** calculated as $\delta_{Zn(L1)2(ClO4)2} - \delta_{L1}$.

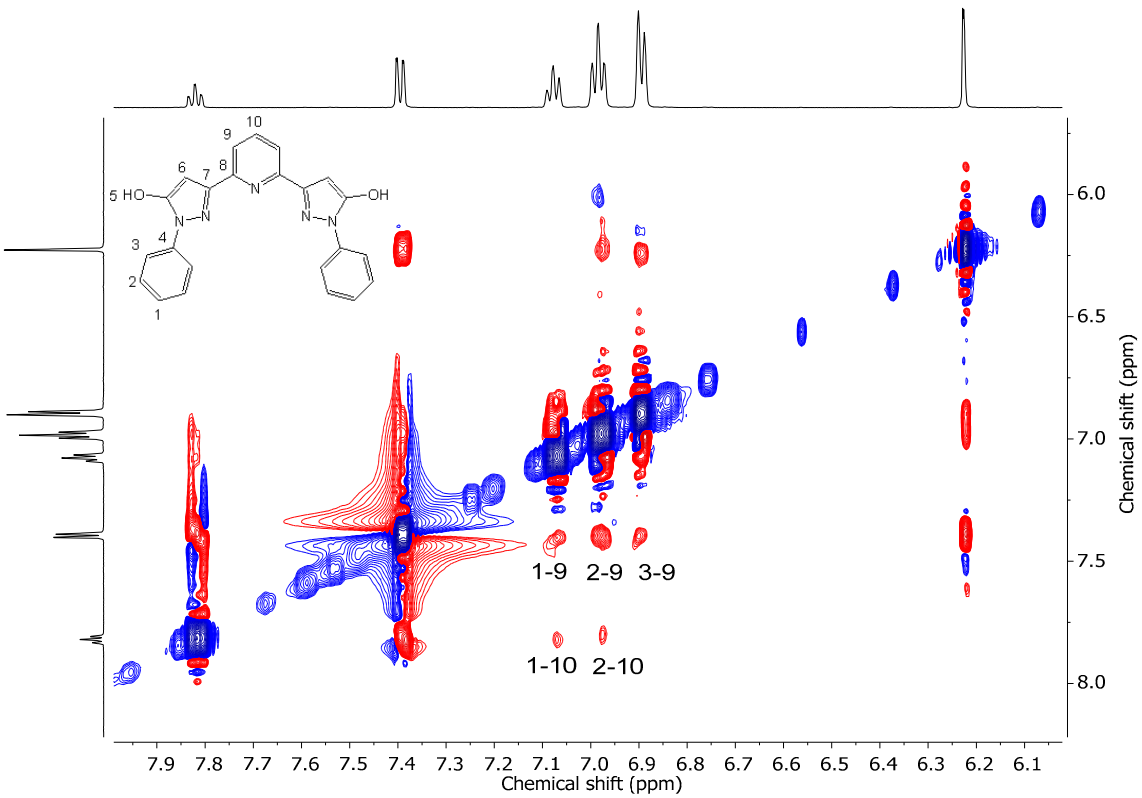

Pair of nuclei	Distance (X-ray)	Cross-peak	Pair of nuclei	Distance (X-ray)	Cross-peak
1-9	4.0 – 4.8	+	1-10	3.8 – 4.0	+
2-9	3.4 – 4.2	+	2-10	4.0 – 5.3	+
3-9	4.5 – 4.8	+	3-10	5.5 – 6.4	–

Figure S11. ROESY NMR data for Zn(**L1**)$_2$(ClO_4)$_2$.

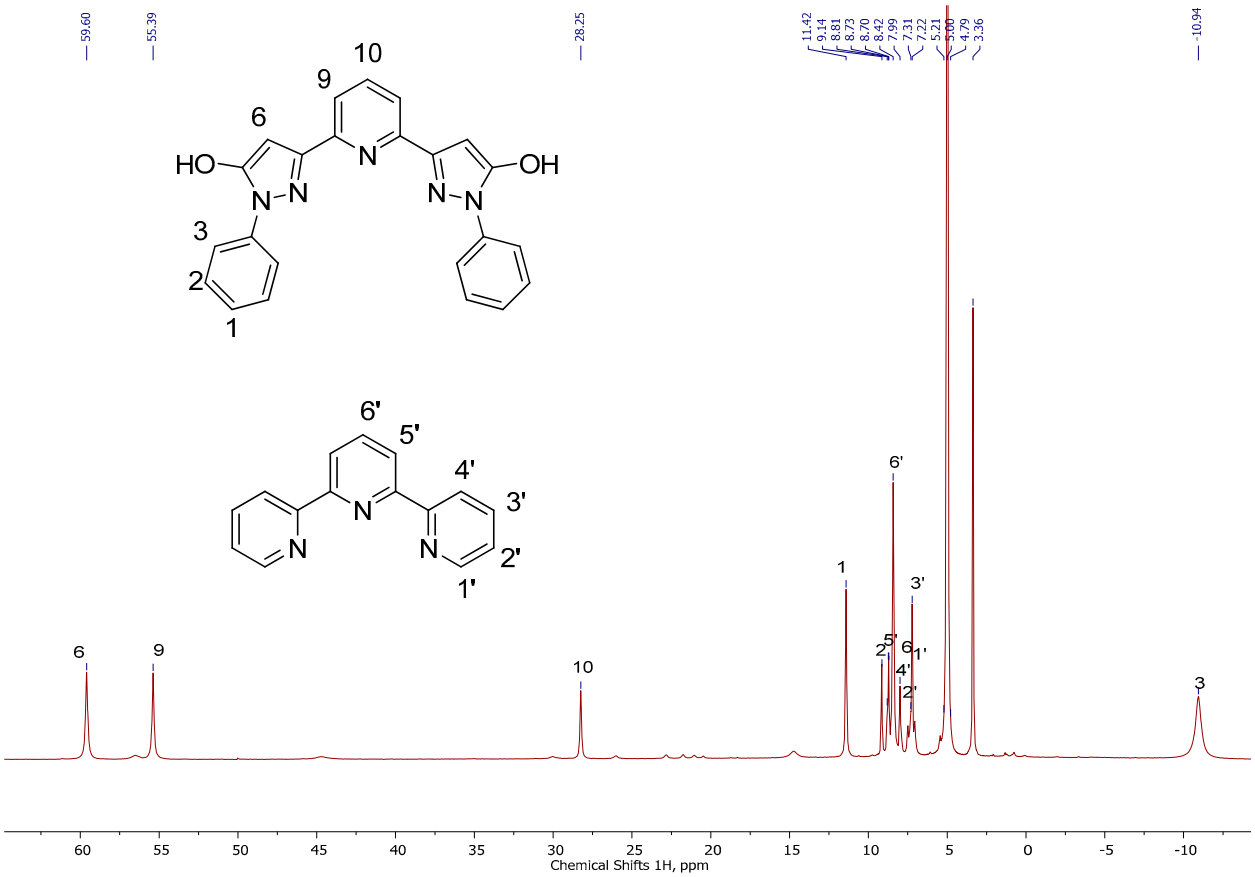

(**a**)

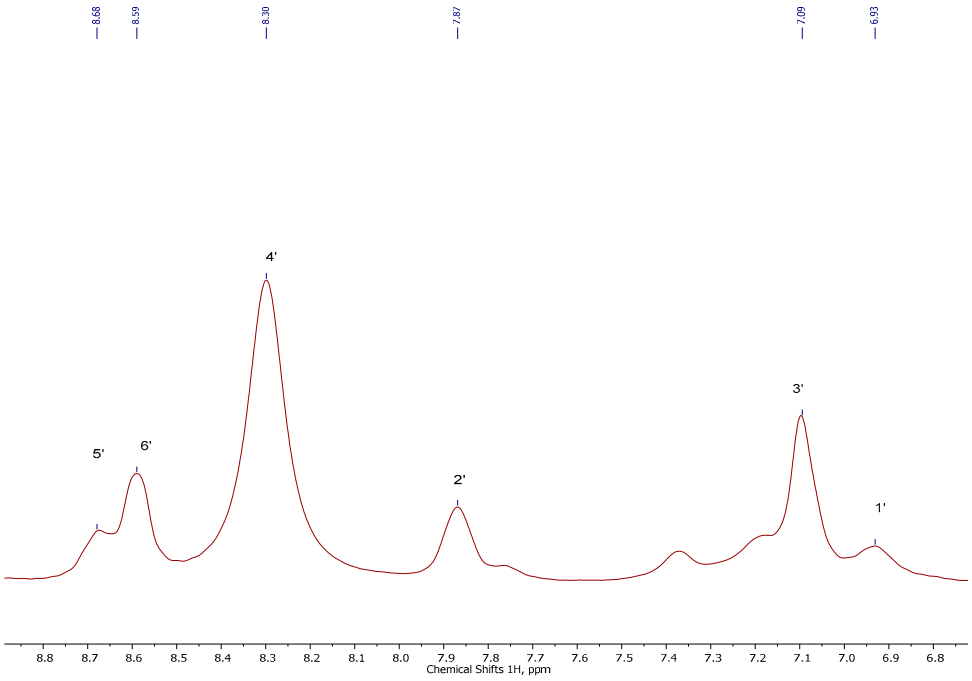

(**b**)

Figure S12. ^{1}H NMR spectra recorded after adding equimolar quantities of **L1**, **terpy** and $FeCl_2$ in methanol-d4 (**a**) and for pure [Fe(**terpy**)$_2$]Cl_2, ^{1}H NMR (300.13 MHz, CD_3OD) δ: 8.68 (4H, br.s., **5'**), 8.59 (2H, br.s., **6'**), 8.30 (4H, br.s., **4'**), 7.87 (4H, br.s., **2'**), 7.09 (4H, br.s., **3'**), 6.93 (4H, br. s., **1'**) (**b**).